ChemPubSoc Europe

DOI: 10.1002/cssc.201701255

CHEMSUSCHEM Full Papers

Non-Aqueous Primary Li–Air Flow Battery and Optimization of its Cathode through Experiment and Modeling

Byoungsu Kim,[a] Kensuke Takechi,[b] Sichao Ma,[a] Sumit Verma,[a] Shiqi Fu,[a] Amit Desai,[a] Ashtamurthy S. Pawate,[a] Fuminori Mizuno,[b, c] and Paul J. A. Kenis*[a]

A primary Li–air battery has been developed with a flowing Li-ion free ionic liquid as the recyclable electrolyte, boosting power capability by promoting superoxide diffusion and enhancing discharge capacity through separately stored discharge products. Experimental and computational tools are used to analyze the cathode properties, leading to a set of parameters that improve the discharge current density of the non-aqueous Li–air flow battery. The structure and configuration of the cathode gas diffusion layers (GDLs) are systematically modified by using different levels of hot pressing and the presence or absence of a microporous layer (MPL). These experiments reveal that the use of thinner but denser MPLs is key for performance optimization; indeed, this leads to an improvement in discharge current density. Also, computational results indicate that the extent of electrolyte immersion and porosity of the cathode can be optimized to achieve higher current density.

Introduction

Lithium ion (Li-ion) batteries have been widely employed in recent and emerging automotive technologies such as electric vehicles (EVs) and hybrid electric vehicles (HEVs).[1] Although car manufacturers such as BMW, Nissan, Tesla, and Toyota have introduced advanced EVs and HEVs, further increases in battery energy density will be critical, most notably to extend the range of next-generation EVs and HEVs. To this end, the focus has been on metal–air batteries because of their high theoretical specific energy densities, that are on par with gasoline.[2] The high specific energy density results from the combination of using high energy alkaline metals as the anode and using oxygen from ambient air as the reactant on the cathode. Several metal–air batteries, such as iron–air, aluminum–air, and zinc–air, have been investigated. Among these, the use of lithium as the anode in lithium–air (Li–air) battery systems has achieved prominence since its conception in 1996.[3]

Li–air batteries hold tremendous potential for storage of renewable energy, as well as for use in mobile devices and EVs,[4] with researchers predicting being able to achieve a 5–10-fold increase in theoretical energy density over the presently used Li-ion batteries. The large theoretical energy density of the Li–air battery is due to the fact that the cathode oxidant O_2 is not stored in the electrode and can be readily obtained from the surrounding environment and the discharge product has significantly high energy density. Furthermore, non-aqueous Li–air batteries are attractive energy storage systems, owing to the aforementioned higher theoretical energy density and their superior stability than, for example, aqueous or hybrid Li–air batteries.[5] However, despite its high energy density, issues such as capacity fading and low current density still need to be overcome.[4a,6] A major cause of these issues is the deposition of discharge products on the surface as well as inside the pores of the cathode, which in turn prevents steady discharge.[6c,7] Multiple approaches to tackle these challenges that are specific to non-aqueous Li–air batteries have been investigated. For example, various non-aqueous electrolytes that improve cycling performance and round-trip efficiency,[8] and different carbon materials and/or substrates that optimize electrodes[9] have been reported.

The cathode, also called the air electrode, is key to achieving high performance non-aqueous Li–air batteries.[10] A gas-diffusion layer (GDL) is an integral part of such a cathode, as it provides control over diffusion-based mass transport while keeping the liquid electrolyte stream and gaseous feed separated. The GDL consists of a carbon fiber substrate (CFS) for support and a micro-porous layer (MPL) that provides the high surface tension necessary to maintain separation between the liquid and gas phases at the liquid–gas-solid interface. GDLs have been studied and optimized previously for a range of electrochemical applications including fuel cells,[11] CO_2 electro-

[a] B. Kim, S. Ma, S. Verma, S. Fu, Dr. A. Desai, Dr. A. S. Pawate, Prof. Dr. P. J. A. Kenis
Department of Chemical and Biomolecular Engineering
University of Illinois at Urbana-Champaign
600 South Mathews Avenue, Urbana, IL 61801 (USA)
E-mail: kenis@illinois.edu

[b] Dr. K. Takechi, Dr. F. Mizuno
Materials Research Department, Toyota Research Institute of North America
1555 Woodridge Avenue, Ann Arbor, MI 48105 (USA)

[c] Dr. F. Mizuno
Toyota Motor Corporation, Higashifuji Technical Center
1200 Mishuku, Susono, Shizuoka 410-1193 (Japan)

Supporting Information and the ORCID identification number(s) for the author(s) of this article can be found under https://doi.org/10.1002/cssc.201701255.

lyzers,[12] and Li–air batteries,[9b,13] but have not been optimized explicitly for a non-aqueous Li–air flow battery.

To further improve performance, several researchers have configured Li–air flow batteries with a flowing aqueous electrolyte on the cathode side while maintaining a non-aqueous electrolyte on the anode side.[14] Use of a flowing aqueous electrolyte on the cathode improves the discharge capacity by continuously supplying dissolved O_2. However, the challenge for this hybrid electrolyte configuration is the identification of a membrane that is compatible with both aqueous and non-aqueous electrolytes. Furthermore, Li–air batteries flowing pre-bubbled non-aqueous electrolyte may provide O_2 more efficiently, but this type of battery cannot avoid intrinsic issues associated with regular Li–air battery such as poor cycling and low power caused by cathode clogging.[15]

Recently, we proposed a new Li–air battery architecture that can decouple the cathode's multiple contradictory functions, electrochemical reactions and discharge product storage, via simple yet drastic changes in the electrolyte composition, completely eliminating Li^+ ions in the area around the cathode using an ionic liquid.[16] The new Li–air battery concept demonstrated continuous discharge similar to fuel cells by storing its discharge product, Li_2O_2, in its bulk electrolyte instead of the cathode surface where Li_2O_2 was found in regular Li–air battery. This concept creates an avenue to redesign Li–air battery systems with flexibility to balance power and capacity independently and efficiently. The discharge product stored in the bulk electrolyte can be decomposed (charged) by the "chemical regeneration" method developed in our group.[17] In the same study, we also reported that the performance of the battery could be improved by stirring the electrolyte because the created convection promoted diffusion of the superoxide anion radical, which is the initial discharge product with a slow diffusion coefficient. Wang and co-workers also developed a similar system using soluble mediators for both discharging and charging processes, and further stored the discharge product, Li_2O_2 resulting from the chemical reaction between the mediators and O_2, in a tank.[18] However, the mediators intrinsically caused voltage efficiency loss, owing to additional electron transfer between the mediators and active materials.

Herein, to improve performance of this new type of Li–air battery, we propose an alternative architecture comprising a flowing electrolyte system using an ionic liquid (Figure 1). By circulating the electrolyte, we expected to boost the power capability by promoting superoxide diffusion and to enhance the discharge capacity by separately storing the discharge products. We also report our experimental and computational investigations on optimizing the discharge behavior of cathodes for a non-aqueous Li–air flow battery. We evaluated GDL parameters that increase discharge current density by varying their structure and composition, specifically by fabricating and evaluating hot-pressed GDLs to improve the discharge current density of Li–air flow batteries. To gain further insights into, and thus optimize the discharge behavior of the cathodes, we performed computational modeling using the commercially available COMSOL multiphysics software package to analyze how different parameters—specifically the properties of the cathode—benefit its performance. Several reports have discussed such simulations for Li–air batteries,[19] but we are not aware of such reports for cathodes of Li–air flow batteries.

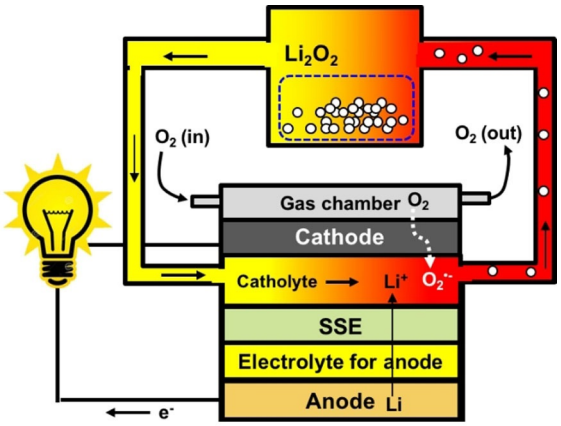

Figure 1. Schematic diagram of the Li–air flow battery. Electrolyte = *N*,*N*-diethyl-*N*-(2-methoxyethyl)-*N*-methylammonium bis(trifluoromethylsulfonyl)imide (DEME–TFSI).

Results and Discussion

Proof of concept and fundamental properties of the Li–air flow battery

Figure 2 shows a schematic depiction of the structure and an actual image of the non-aqueous Li–air flow battery used in this study. Discharge profiles of the new structure Li–air battery with and without electrolyte flowing at 0.077 mA cm^{-2} of constant current density are shown in Figure 3. The discharge potentials for both static and flow batteries are relatively low (around 2 V) compared to other reported Li–air flow batteries,[14,15] owing to the relatively large overpotential caused by the low diffusivity of O_2^- in catholyte that lacks Li salt. The clear advantage of the flowing system is evident from the steady profile around 2.0 V of discharge voltage. This indicates that the initial discharge product, superoxide anion radical $O_2^{\cdot-}$, was effectively removed from the cathode surface and transported into the bulk electrolyte by mechanical flow of the electrolyte. In the case of static electrolyte, the slow diffusion of $O_2^{\cdot-}$ cannot keep up with electrochemical reduction of O_2 and caused a large concentration overpotential, as evident from the discharge profile as a rapid drop in voltage. This result demonstrates the benefit of using a flowing electrolyte in the new system. The inset photographs in Figure 3 show a clear change in the electrolyte appearance before and after discharge. Moreover, a movie from the experiment showing this change in electrolyte appearance can be found in the Supporting Information. The generated final product (white precipitate in the electrolyte) was identified as Li_2CO_3 by Raman spectroscopy (Figure S1 in the Supporting Information). As dried air containing a slight amount of moisture and CO_2 was introduced in the battery here, the discharge product starting from $O_2^{\cdot-}$ will be transformed to Li_2CO_3 through the reactions given by Equations (1), (2), (3), and (4), which was confirmed

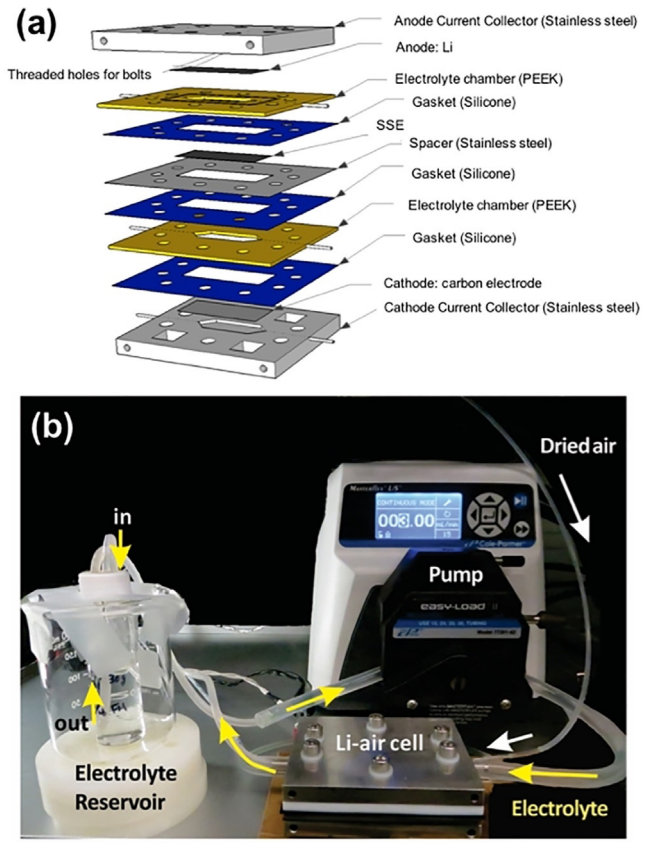

Figure 2. Experimental design and setup of the Li–air flow battery. a) Perspective view schematic of the cell and b) actual photograph of the non-aqueous Li–air flow battery consisting of current collectors for the anode and cathode, a Li metal anode, a GDE as cathode, a gasket, chambers for anolyte and catholyte, a solid-state electrolyte (SSE), and a stainless steel spacer for the SSE.

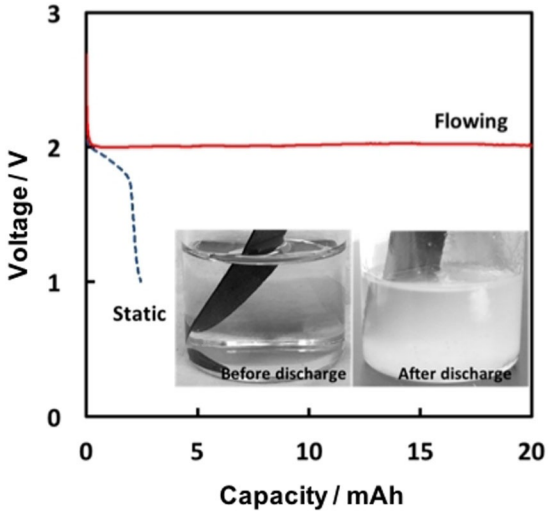

Figure 3. Discharge behavior of non-aqueous Li–air battery with and without flowing catholyte.

by a separate model experiment by exposing Li_2O_2 in air (Figure S2). Note that the direct reaction between Li_2O_2 and CO_2, which is a possible pathway to generate Li_2CO_3 from Li_2O_2, can be ruled out, as explained in our previous study.[20] For practical usage of this device, the supplied gas should be completely dried and decarbonated to give Li_2O_2 as the discharge product, similar to what occurs in a regular Li–air battery. In principle, because Li_2O_2 or Li_2CO_3 generation occurs in the bulk electrolyte and does not affect any electrochemical reaction or cathode performance, consistency with operation of a regular Li–air battery is maintained in the cathode optimization study.

$$O_2^{\cdot-} + Li^+ \rightarrow LiO_2^{\bullet} \quad (1)$$

$$2LiO_2^{\bullet} \rightarrow Li_2O_2 + O_2 \quad (2)$$

$$Li_2O_2 + H_2O \rightarrow 2LiOH + {}^1/_2\ O_2 \quad (3)$$

$$2LiOH + CO_2 \rightarrow Li_2CO_3 + H_2O \quad (4)$$

Effect of the presence/absence of MPL on Li–air flow battery performance

Optimizing electrodes is key for improving the discharge current density of non-aqueous Li–air battery.[10b] To optimize the discharge current density of the Li–air flow battery, we modified structure and surface of GDLs of the cathodes. First, the discharge profiles of the flow batteries assembled with two commercially available GDLs, TGP-H-120 and Sigracet 35 BC, were compared to investigate the effect of MPL on discharge current density and electrolyte flooding. TGP-H-120 has a CFS, but no MPL, while Sigracet 35 BC has a CFS as well as a MPL loaded with 5 wt% PTFE. The Li–air flow battery with TGP-H-120 achieved a continuous discharge current density of 0.013 mA cm^{-2} at 2.1 V, whereas the same configuration with Sigracet 35 BC produced a six times higher current density of 0.077 mA cm^{-2} (Figure 4). These results highlight the importance of the MPL in preventing flooding of the electrode (liquid electrolyte seeping through the cathode). Also note that the observed higher current densities allowed for more rapid evaluation of battery performance. The theoretical

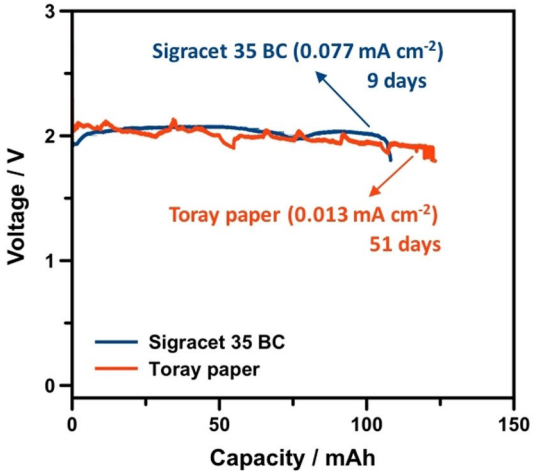

Figure 4. Voltage profile with GDLs with MPLs (Sigracet 35 BC) and GDLs without MPLs (TGP-H-120) in the Li–air flow battery.

energy density of the system was calculated to be 500–1500 Wh L^{-1} (Figure S3); It depends on the balance between the volume of the electrolyte reservoir and the electrode assembly. The power and capacity can also be modified by changes to the reactor and/or the dissolved species in the electrolytes. Indeed, the concept offers high flexibility with respect to battery design.

Effect of hot-pressed GDLs on Li–air flow battery performance

The two GDLs tested above (Figure 4) were prone to flooding, which hampers battery performance by limiting O_2 diffusion. To decrease the thickness of the GDL and to make the MPL denser, and hopefully less prone to flooding, we compressed multiple Sigracet 35 BC GDLs by hot-pressing at elevated temperature, typically 125 °C. Table 1 shows the details of the GDLs fabricated in this study. In battery testing those with the GDLs fabricated under a compression pressure of 2268 kgf (GDL#H-4) performed the best (the highest current density; Figure 5). Hot pressing will result in thinner but denser CFS and MPL layers. A thinner CFS will shorten the diffusion distance for O_2, while a thinner, denser (so less porous) MPL will increase the resistance of the GDL towards flooding (increased surface tension) which in turn helps to define better the position of the 3-phase boundary layer near or inside MPLs, not near CFSs, allowing continuous O_2 diffusion, which potentially further enhances the discharge current density of the Li–air flow battery studied here (see also the prior section).

Table 1. Physical properties, composition and fabrication method of GDLs.

Name	Sample description	Substrate	Method	CP[a] [kgf]
GDL#H-1	Hot-pressed GDLs	Sigracet 35 BC	Hot pressing	227
GDL#H-2				680
GDL#H-3				1360
GDL#H-4				2268
GDL#H-5				4536
GDL#1	GDL without MPL	Toray-H-120	–	–
GDL#2	GDL with MPL	Sigracet 35 BC	–	–

[a] CP = compression pressure.

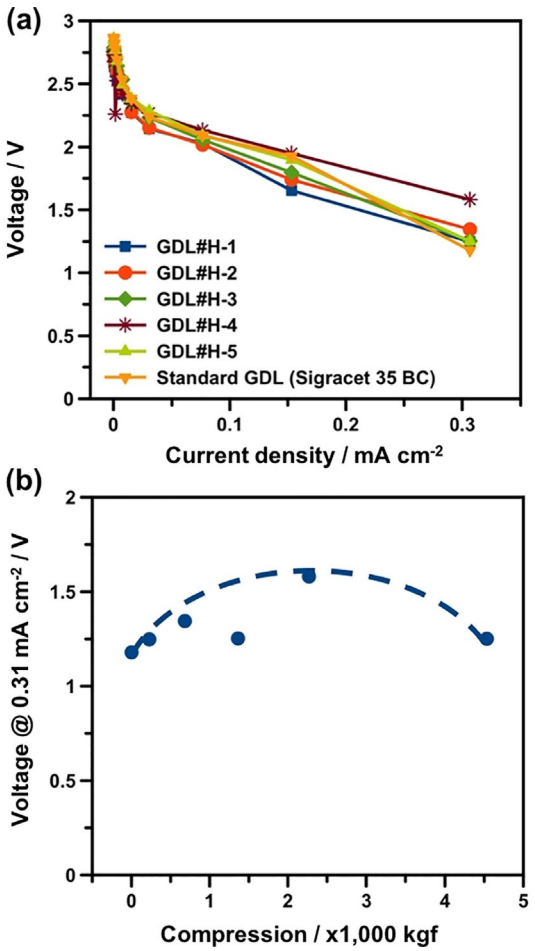

Figure 5. a) Voltage profile as a function of discharge current density with GDLs made with different compression pressures in the Li–air flow battery. b) Discharge voltage as a function of compression pressure at a discharge current density of 0.31 mA cm^{-2}.

Prior work on GDLs for fuel cells has shown that not only the thickness but also the porosity and/or permeability of the GDLs change upon applying different compression pressures during assembly of cells.[21] Whereas the diffusion path for reactants becomes shorter for electrodes prepared with higher compression pressures, the overall pore volume and gas permeability of the GDL also decreases, which may limit mass transport. Furthermore, excessive compression of GDLs for fuel cells can also lead to a drop in performance due to limited mass transport[21a] and/or due to structural damage of the GDL.[21c,22] For example, Chang et al. reported previously that compressing a GDL to half of its initial thickness decreased gas permeability to one-tenth of its initial value.[21a] Also, compression of GDLs during the assembly is known to increase conductivity of GDLs and decrease the contact resistance between the GDL and other components, leading to better performance for fuel cells.[21a,b,23] However, for our Li–air flow battery, we used the same gasket when testing the GDLs fabricated under different compression pressures and we applied the same clamping pressure to assemble the battery. Hence, we expect the contact resistance to be the same for each cell.

To assess which factors affect battery performance, we characterized the porosity and thickness of GDLs. SEM images and actual thickness/porosity of GDLs fabricated under different compression pressures are shown in Figures S4 and S5, respectively. SEM data shows that the thickness of the MPLs decreased from 80.3 to 30.1 μm upon increasing the compression pressures from 0 to 4536 kgf, while the thickness of the CFSs decreased from 200.8 to 134.5 μm (Figure S5 a). Micro-CT experiments followed by data analysis shows that the GDL porosity decreases with increasing compression pressure, with the lowest porosity observed for GDLs prepared at 2268 kgf (Figure S5 b) coinciding with the highest discharge current density.

Indeed, different factors resulting from the application of different compression levels play an important role with respect to Li–air flow battery performance. Optimum performance is expected for a certain compression pressure (2268 kgf in this case) due to a tradeoff between (1) better control over electrolyte (preventing flooding) and/or a better defined position of the 3-phase boundary layer upon reducing porosity of the MPL, and (2) mass transport of oxygen to the catalytic interface. Furthermore, Micro-CT analysis of GDLs prepared by hot-pressing at 4536 kgf revealed that carbon fibers from the CFS start to intrude into the MPL causing structural damage that may accelerate electrolyte flooding (Figure S5 b), which in turn may cause precipitation of Li_2O_2 inside the pores of the cathode. Indeed, in our experiments, this precipitation eventually terminated the discharge process of the Li–air flow battery, indicating the importance of preventing electrolyte flooding for Li–air flow batteries.

Developing a model for the Li–air flow battery

Model configuration

To further understand and estimate the behavior of the Li–air flow battery, we created a Li–air battery model in COMSOL. Figure 6 a and b show schematic diagrams of the Li anode, the electrolyte and the GDL-based cathode used in the experimental battery configuration, as well as the schematic of the configuration used to model this Li–air flow battery, respectively. In brief, the Li–air flow battery model used here is based on a Li–air static battery model provided by COMSOL, originating from prior work.[19b] Starting from this Li–air static battery configuration,[19b] the only difference is that a solid-state electrolyte (SSE) is used for the Li–air flow battery model, instead of a polymer separator. The cell configuration for the Li–air flow battery model is comprised of a metal lithium anode, a solid-state electrolyte, and a porous cathode (Figure 6 b). Specifically, we used this model to determine optimal parameters for GDLs (porosity, and depth of immersion of the cathode by electrolyte) to estimate the maximum possible current density that can be achieved for a given configuration. Electrochemical reduction of O_2 occurs on the surface of the GDL within the GDL, but generally close to the three-phase boundary, the intersection of the electrolyte, the gas phase, and the GDL surface. Depending on the extent of electrolyte penetration into the GDL, the O_2 has to diffuse through a smaller or larger fraction of the porous GDL to reach the three-phase interface where it can react with Li^+ from the electrolyte. Operated under two conditions: the absence and presence of Li_2O_2 precipitation due to a flowing or static electrolyte, respectively. Rather than have a flowing electrolyte layer as part of the model configuration, we made certain assumptions with respect to Li_2O_2 solubility to simplify the model.

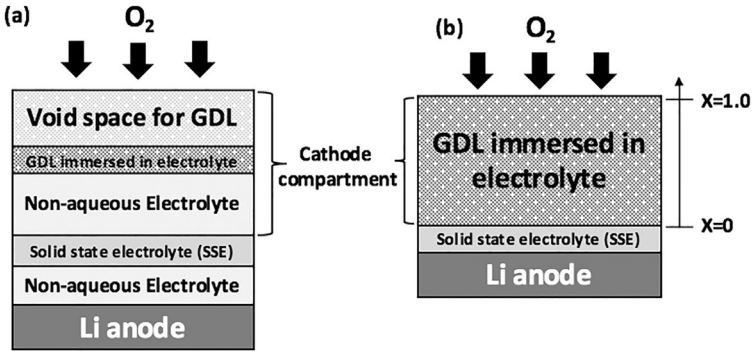

Figure 6. Schematic diagram of the Li anode, the electrolyte, and the GDL-based cathode: a) for the actual experimental battery configuration; b) for the configuration used to model this Li–air flow battery.

Assumptions

We implemented the following assumptions to obtain information from the model on how GDL porosity and the depth of cathode immersion in electrolyte affect performance:

1)
The Li_2O_2 is the main reaction product and is only formed inside the porous cathode.

2)
To model the flowing electrolyte condition, the solubility of Li_2O_2 in the electrolyte is assumed to approach infinity (1 000 000 mol m^{-3}), whereas a solubility of 0.09 mol m^{-3} is used for the non-flowing conditions.

3)
The concentration of cation in model is considered as the concentration of DEME + (3300 mol m^{-3}).

4)
The Li–air cell is operated under isothermal conditions.

With these assumptions, specifically by assuming a very high solubility for Li_2O_2, we ensure that the behavior of the Li–air flow battery is not limited by Li_2O_2 precipitation and subsequent clogging of pores within the cathode. In other words, the model seeks to identify maximum achievable performance levels in the absence of Li_2O_2 precipitation issues.

Comparison of the Li–air flow battery model with experimental results

We simulated the Li–air flow battery and compared the modeling results to the experimental results with respect to two parameters: discharge capacity and discharge current density. Model of Li–air battery is investigated under condition of flowing electrolyte and non-flowing electrolyte. The discharge in the non-flowing case was terminated by a continuous growth of solid Li_2O_2 inside the porous cathode (Figure 7 a), which predominantly led to a lowering of the porosity (Figure 7 b). In other words, the pore-blocking effect of Li_2O_2 deposition is apparent in our results for the non-flowing case, in agreement with our experimental work (Figure 3). However, the same configuration with the electrolyte flowing exhibits a substantial increase in specific capacity compared

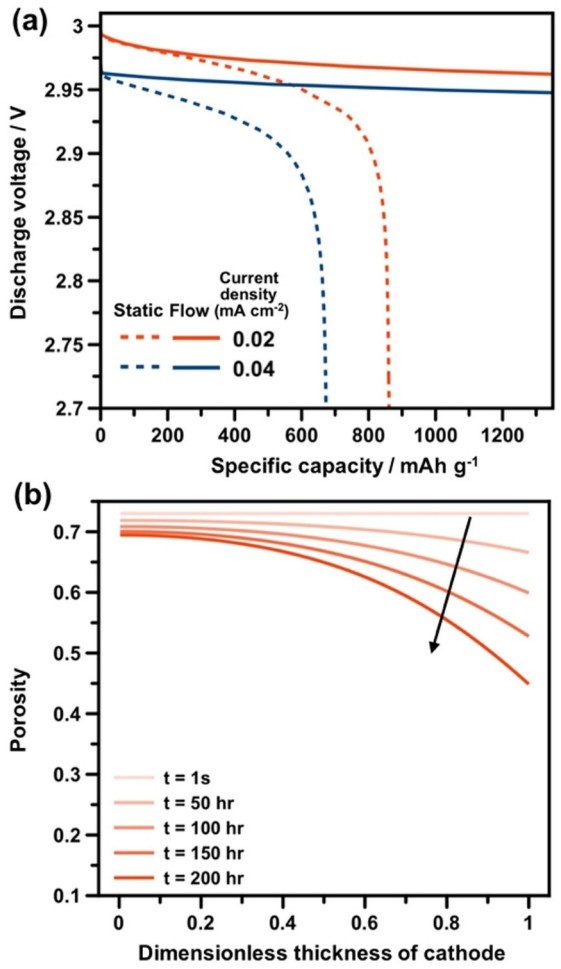

Figure 7. a) Voltage–discharge capacity curves for different applied current densities (0.02 and 0.04 mA cm^{-2}) obtained from simulation of the Li–air battery under static (dashed line) and flowing (solid line) electrolyte operation conditions. b) Simulation results of the gradual drop of porosity in the cathode over time in the absence of electrolyte flow when operating the battery at 0.02 mA cm^{-2}.

with the non-flowing case (Figure 7a). The flowing electrolyte drastically reduced the extent of clogging of the pores in the cathode by continuously removing the discharge product and thus allows the battery to continue operation for a longer time. We further examined the discharge behavior of the same configuration operated with a flowing or non-flowing electrolyte at different discharge current densities. An increase in the discharge current density was observed that can be correlated to a decrease in the discharge voltage in both the flowing and non-flowing case.

Next, we compared the above results from the model with our experimental data. Note that the discharge voltages as obtained from the model (Figure 7) are much higher than the experimentally observed discharge voltages (Figure 3). This difference is due to the higher contact resistance caused by the thick electrolyte chamber and SSE, aspects that are not included in the model. In summary, the trends of discharge voltage and discharge capacity apparent in the modeling results are consistent with the trends observed experimentally (Figure 3), suggesting that our model is suitable for determining optimal parameters of cathodes for non-aqueous Li–air flow batteries.

Determining the maximum current density by optimizing cathode structure in COMSOL

Next, we used our aforementioned Li–air flow battery model to gain further insight on how to optimize cathode performance. Specifically, to identify optimum cathode porosity and optimum depth of immersion of the cathode by electrolyte, we systematically varied the depth of electrolyte immersion between 10 and 200 μm, and we varied the porosity between 0.1 and 0.9. The sequence to estimate the maximum discharge current density and optimal depth of electrolyte immersion is shown in Figure S6. In brief, the discharge current density is increased until the discharge process terminates where the discharge voltage drops dramatically (Figure S6a). Next, discharge current density is plotted as a function of discharge voltage except for the value of discharge current density where the discharge process terminates (Figure S6b), and only the highest current density is plotted as a function of depth of immersion of the cathode by electrolyte (Figure S6c). This process is repeated for different initial concentrations of O_2, as well as for different depths of electrolyte immersion in the cathode.

The maximum discharge current density as a function of porosity of the cathode and as a function of depth of immersion of the cathode by electrolyte with different initial concentrations of O_2 is shown in Figure 8. The maximum current density that can be achieved increases with increasing porosity of the cathode (Figure 8a). This trend indicates that higher porosity improves O_2 transport and also could provide a large free volume for Li_2O_2. However, in such a flow cell, to achieve optimum performance without the occurrence of electrode flooding, pressure balance across the GDLs between the liquid electrolyte stream and the gaseous O_2 feed needs to be maintained. For example, prior work has shown that a sufficiently low porosity of the GDL surface will help to prevent electrode flooding for flow cells.[12b] Therefore, an increase in porosity beyond a certain point would lead to flooding of the cathode, suggesting that optimization of cathode porosity would enable achieving a suitable tradeoff between maximizing O_2 transport while preventing electrolyte flooding.

The depth of immersion of the cathode by electrolyte also plays an important role in determining the discharge current density for the Li–air flow battery. Discharge voltages for discharge current densities with different initial concentrations of O_2 and depth of immersion are shown in Figure S7. A different trend was observed for maximum discharge current density as a function of depth of immersion (Figure 8b) compared with the results obtained as a function of porosity (Figure 8a). Maximum discharge current density is observed at depths of cathode immersion of 30, 50, and 70 μm for an initial O_2 concentrations of 5, 15, and 20 mol m^{-3}, respectively (Figure 8b). These results can be attributed to the slow diffusion of O_2, $DEME^+$, and the discharge product, $O_2^{\cdot-}$, in the electrolyte. This observation suggests that an optimum depth of cathode immersion

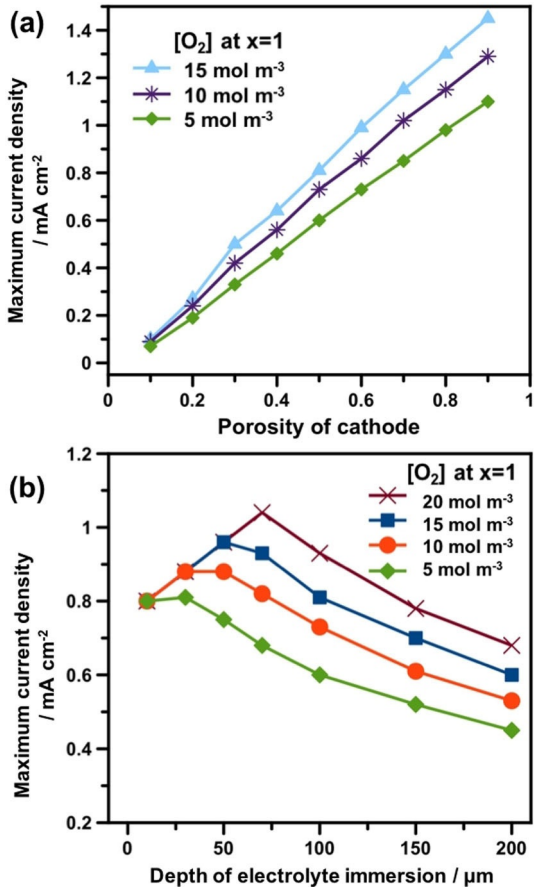

Figure 8. Simulation results of maximum current density that can be achieved as a function of a) cathode porosity, ranging from 0.1 to 0.9 and b) depth of cathode immersion, ranging from 10 to 200 µm for different initial concentrations of O_2 (5, 10, 15 and 20 mol m^{-3}) in DEME–TFSI (3300 mol m^{-3} of $DEME^+$).

is key to maximize current density for different operating conditions. Note that all data achieved in this modeling work can be found in Table S1.

Conclusion

Herein we have introduced the concept of a Li–air battery with a flowing non-aqueous electrolyte (DEME–TFSI in this work) and developed an actual reactor based on a flow cell design similar to fuel cell or CO_2 electrolyzer. These optimized Li–air flow batteries improve the discharge capacity due to promoted superoxide diffusion and separately stored discharge products. Also, the experiments and modeling efforts provide insight regarding the structure of cathodes that lead to the best performance for Li–air flow batteries. Through experiments, the structure and surface (specifically the presence or absence of a microporous layer, MPL) of the cathode was optimized for producing higher discharge current density. Hot-pressed GDLs exhibited improved discharge current density, which can be attributed to a denser MPL with an intact 3-phase boundary layer structure that prevents electrode flooding. In addition, through modeling we analyzed how different parameters for cathodes, specifically the porosity and the depth of electrolyte immersion of the cathode, benefit the performance of the non-aqueous Li–air flow battery. Through simulations of a Li–air flow battery model in COMSOL we are able to predict the flow battery's discharging behavior, estimate the maximum current density that can be achieved, and determine a set of parameters for the electrode that optimizes performance. Indeed, simulation results revealed the importance of optimizing the cathode of the Li–air flow battery for different operating conditions.

Experiments and modeling efforts made here for a non-aqueous Li–air flow battery, as well as for its cathode, confirmed that the flow configuration with electrode optimization could improve not only the discharge capacity but also the current density of the Li–air flow battery. These many interesting findings and recent discoveries in this field provide insight for further optimization of reactor configuration and/or electrode before commercialization of the non-aqueous Li–air flow battery becomes feasible. Specifically, further improvement in the battery performance could be achieved by investigating the effect of different carbon materials (composition and morphology) for cathodes. Moreover, extensive durability tests of the electrodes and their performances during multiple charging–discharging cycles will also need to be performed.

Experimental Section

Preparation of carbon cathode

Table 1 shows the details of the GDLs fabricated in this study. For comparison, Sigracet 35 BC (SGL Technologies) and TGP-H-120 (Toray corp.) were used to determine the effect of MPL in Li–air flow batteries. Sigracet 35 BC is a GDL comprised of 5 wt% polytetrafluoroethylene (PTFE)-treated carbon paper and a teflonized MPL, whereas TGP-H-120 is a GDL comprised of 10 wt% PTFE-treated carbon fiber without MPL. The GDL#H samples are hot pressed (Carver 3851-0) Sigracet 35 BC at various compression pressures (0, 227, 680, 1360, 2268, and 4536 kgf) at a temperature of 125 ± 5 °C for 5 min.

Li–air flow cell assembly and its use for electrode testing

A schematic structure and actual image of the non-aqueous Li–air flow battery used in this study are shown in Figure 2. Briefly, two stainless steel plates (10.0 × 8.0 × 1.0 cm) serving as current collectors hold the flow cell together by using ten stainless steel bolts and provide electrical contact between the electrodes and an external potentiostat. PTFE insulation around the bolts prevented any potential short-circuits at the contact areas with current collectors. The cathode current collector has a 2.0 cm × 4.0 cm window with 0.1 cm depth behind the GDL to allow for the flow of air or other gases. The anode current collector also has a 2.0 cm × 4.0 cm window with < 0.2 mm depth to accommodate the Li metal foil (FMC Lithium Corp., USA). Two 2 mm-thick polyether ether ketone (PEEK) spacers with 2.0 cm × 4.0 cm windows provide the catholyte and anolyte flow areas, respectively. A solid-state electrolyte (SSE; LIC-GC, Ohara Corp.; 2.5 cm × 5.0 cm × 180 µm) surrounded by PEEK is inserted between the catholyte and anolyte chambers. The cathode is a 2.3 cm × 4.5 cm GDL sandwiched between the cathode current collector and the catholyte chamber. As the electrolyte, *N*,*N*-diethyl-*N*-(2-methoxyethyl)-*N*-methylammonium bis(trifluoro-

methylsulfonyl)imide (DEME–TFSI; Kanto Corp., USA), was flowed through the catholyte chamber with dried air (1–2% RH) flowing through the gas chamber at 7 SCCM. The electrolyte was supplied by a peristaltic pump, Masterflex L/S(Cole-Parmer, USA), with a flow rate of 5 mL min^{-1}. 1 M LiTFSI dissolved in propylene carbonate (Kishida Chemical Corp., Japan) was used as an electrolyte for anode side (not flowed in this study).

Before performing electrochemical evaluation including battery performance test, the cell was kept at the operating temperature (25 °C) for 5 h, and saturation of O_2 in the IL electrolyte was obtained and confirmed by a steady open circuit voltage. The actual electrochemical measurements were performed using a model MCV cycle life test equipment (Bitrode Corp., USA). The current–voltage (*I–V*) tests were conducted by using a current holding time of 30 min at current densities from 0.0001 to 0.3 mA cm^{-2}. The constant discharge test was conducted by using a fixed current density of 0.013 or 0.077 mA cm^{-2}.

Structural characterization of GDLs

The thicknesses of the GDLs were characterized by using SEM. Cross-sectional images of samples were obtained by using SEM (Philips XL30 ESEM-FEG) with an acceleration voltage of 10.0 kV and a spot size of 3.0 nm, resulting in a magnification of 1300. To measure the porosity of the GDLs, images of the structural features of the GDLs over an area of several square millimeters were obtained using Micro-CT (Micro-XCT 400, Xradia) with an X-ray source at 40 kV and a current of 200 μA, as in our prior work.[24] The images were then processed to reconstruct 2D radiographic cross-sectional image stacks and 3D tomographic virtual models of the GDL. The initial reconstruction of MicroCT data was carried out by using TXM Re-constructor software (Xradia). Further image processing was performed by using the Amira visualization software package (Version 5.3, Visage Imaging) for subsequent quantitative analysis of the GDL microstructure. Detailed descriptions of porosity measurement procedures can be found in our previous work.[24]

Acknowledgements

The authors thank Y. Hase (Toyota Central R&D Labs., Inc.), T. Arthur and N. Singh (TRINA) for fruitful discussion and J. Karz (University of Montana) for COMSOL simulation.

Conflict of interest

The authors declare no conflict of interest.

Keywords: batteries · electrodes · ionic liquids · lithium · modeling

[1] E. J. Cairns, P. Albertus in *Annual Review of Chemical and Biomolecular Engineering, Vol. 1* (Eds.: J. M. Prausnitz, M. F. Doherty, R. A. Segalman), Annual Reviews, Palo Alto, CA, **2010**, pp. 299–320.

[2] a) F. Y. Cheng, J. Chen, *Chem. Soc. Rev.* **2012**, *41*, 2172–2192; b) J. S. Lee, S. T. Kim, R. Cao, N. S. Choi, M. Liu, K. T. Lee, J. Cho, *Adv. Energy Mater.* **2011**, *1*, 34–50.

[3] K. M. Abraham, Z. Jiang, *J. Electrochem. Soc.* **1996**, *143*, 1–5.

[4] a) G. Girishkumar, B. McCloskey, A. C. Luntz, S. Swanson, W. Wilcke, *J. Phys. Chem. Lett.* **2010**, *1*, 2193–2203; b) A. Kraytsberg, Y. Ein-Eli, *J. Power Sources* **2011**, *196*, 886–893; c) P. G. Bruce, S. A. Freunberger, L. J. Hardwick, J. M. Tarascon, *Nat. Mater.* **2012**, *11*, 19–29; d) J. Christensen, P. Albertus, R. S. Sanchez-Carrera, T. Lohmann, B. Kozinsky, R. Liedtke, J. Ahmed, A. Kojic, *J. Electrochem. Soc.* **2012**, *159*, R1–R30; e) D. S. Geng, N. Ding, T. S. A. Hor, S. W. Chien, Z. L. Liu, D. Wuu, X. L. Sun, Y. Zong, *Adv. Energy Mater.* **2016**, *6*, 1502164.

[5] a) J. Lu, L. Li, J. B. Park, Y. K. Sun, F. Wu, K. Amine, *Chem. Rev.* **2014**, *114*, 5611–5640; b) A. C. Luntz, B. D. McCloskey, *Chem. Rev.* **2014**, *114*, 11721–11750; c) R. Black, B. Adams, L. F. Nazar, *Adv. Energy Mater.* **2012**, *2*, 801–815.

[6] a) F. J. Li, T. Zhang, H. S. Zhou, *Energy Environ. Sci.* **2013**, *6*, 1125–1141; b) L. Grande, E. Paillard, J. Hassoun, J. B. Park, Y. J. Lee, Y. K. Sun, S. Passerini, B. Scrosati, *Adv. Mater.* **2015**, *27*, 784–800; c) R. Padbury, X. W. Zhang, *J. Power Sources* **2011**, *196*, 4436–4444.

[7] a) S. S. Zhang, D. Foster, J. Read, *J. Power Sources* **2010**, *195*, 1235–1240; b) V. Viswanathan, K. S. Thygesen, J. S. Hummelshoj, J. K. Norskov, G. Girishkumar, B. D. McCloskey, A. C. Luntz, *J. Chem. Phys.* **2011**, *135*, 214704.

[8] a) K. Takechi, Y. Kato, Y. Hase, *Adv. Mater.* **2015**, *27*, 2501–2506; b) H. Nakamoto, Y. Suzuki, T. Shiotsuki, F. Mizuno, S. Higashi, K. Takechi, T. Asaoka, H. Nishikoori, H. Iba, *J. Power Sources* **2013**, *243*, 19–23; c) B. D. McCloskey, A. Valery, A. C. Luntz, S. R. Gowda, G. M. Wallraff, J. M. Garcia, T. Mori, L. E. Krupp, *J. Phys. Chem. Lett.* **2013**, *4*, 2989–2993; d) B. D. McCloskey, D. S. Bethune, R. M. Shelby, T. Mori, R. Scheffler, A. Speidel, M. Sherwood, A. C. Luntz, *J. Phys. Chem. Lett.* **2012**, *3*, 3043–3047.

[9] a) C. Tran, X. Q. Yang, D. Y. Qu, *J. Power Sources* **2010**, *195*, 2057–2063; b) L. Xu, J. Ma, B. H. Li, F. Y. Kang, *J. Power Sources* **2014**, *255*, 187–196; c) M. M. Ottakam Thotiyl, S. A. Freunberger, Z. Peng, P. G. Bruce, *J. Am. Chem. Soc.* **2013**, *135*, 494–500.

[10] a) M. K. Song, S. Park, F. M. Alamgir, J. Cho, M. L. Liu, *Mater. Sci. Eng. R* **2011**, *72*, 203–252; b) Z. Y. Wen, C. Shen, Y. Lu, *ChemPlusChem* **2015**, *80*, 270–287; c) Z. Ma, X. X. Yuan, L. Li, Z. F. Ma, D. P. Wilkinson, L. Zhang, J. J. Zhang, *Energy Environ. Sci.* **2015**, *8*, 2144–2198.

[11] a) G.-G. Park, Y.-J. Sohn, T.-H. Yang, Y.-G. Yoon, W.-Y. Lee, C.-S. Kim, *J. Power Sources* **2004**, *131*, 182–187; b) W.-M. Yan, C.-Y. Hsueh, C.-Y. Soong, F. Chen, C.-H. Cheng, S.-C. Mei, *Int. J. Hydrogen Energy* **2007**, *32*, 4452–4458; c) G. Y. Lin, T. Van Nguyen, *J. Electrochem. Soc.* **2005**, *152*, A1942–A1948; d) J. F. Lin, J. Wertz, R. Ahmad, M. Thommes, A. M. Kannan, *Electrochim. Acta* **2010**, *55*, 2746–2751.

[12] a) H.-R. M. Jhong, F. R. Brushett, P. J. A. Kenis, *Adv. Energy Mater.* **2013**, *3*, 541–541; b) B. Kim, F. Hillman, M. Ariyoshi, S. Fujikawa, P. J. A. Kenis, *J. Power Sources* **2016**, *312*, 192–198.

[13] a) H. Cheng, K. Scott, *J. Power Sources* **2013**, *235*, 226–233; b) H. Geaney, J. O'Connell, J. D. Holmes, C. O'Dwyer, *J. Electrochem. Soc.* **2014**, *161*, A1964–A1968.

[14] a) P. He, Y. G. Wang, H. S. Zhou, *Electrochem. Commun.* **2010**, *12*, 1686–1689; b) J. P. Zheng, P. Andrei, M. Hendrickson, E. J. Plichta, *J. Electrochem. Soc.* **2011**, *158*, A43–A46; c) X. J. Chen, A. Shellikeri, Q. Wu, J. P. Zheng, M. Hendrickson, E. J. Plichta, *J. Electrochem. Soc.* **2013**, *160*, A1619–A1623.

[15] L. Grande, A. Ochel, S. Monaco, M. Mastragostino, D. Tonti, P. Palomino, E. Paillard, S. Passerini, *Energy Technol.* **2016**, *4*, 85–89.

[16] K. Takechi, N. Singh, T. S. Arthur, F. Mizuno, *ACS Energy Lett.* **2017**, *2*, 694–699.

[17] Y. Hase, J. Seki, T. Shiga, F. Mizuno, H. Nishikoori, H. Iba, K. Takechi, *Chem. Commun.* **2016**, *52*, 12151–12154.

[18] a) Y. G. Zhu, C. Jia, J. Yang, F. Pan, Q. Huang, Q. Wang, *Chem. Commun.* **2015**, *51*, 9451–9454; b) Y. G. Zhu, X. Wang, C. Jia, J. Yang, Q. Wang, *ACS Catal.* **2016**, *6*, 6191–6197.

[19] a) P. Andrei, J. P. Zheng, M. Hendrickson, E. J. Plichta, *J. Electrochem. Soc.* **2010**, *157*, A1287–A1295; b) U. Sahapatsombut, H. Cheng, K. Scott, *J. Power Sources* **2013**, *227*, 243–253; c) R. Younesi, M. Hahlin, F. Bjorefors, P. Johansson, K. Edstrom, *Chem. Mater.* **2013**, *25*, 77–84; d) T. Dabrowski, A. Struck, D. Fenske, P. Maass, L. C. Ciacchi, *J. Electrochem. Soc.* **2015**, *162*, A2796–A2804; e) L. H. Ye, W. Q. Lv, K. H. L. Zhang, X. N. Wang, P. F. Yan, J. H. Dickerson, W. D. He, *Energy* **2015**, *83*, 669–673; f) K. Yoo, A. Deshpande, S. Banerjee, P. Dutta, *Electrochim. Acta* **2015**, *176*, 301–310.

[20] K. Takechi, T. Shiga, T. Asaoka, *Chem. Commun.* **2011**, *47*, 3463–3465.

[21] a) W. R. Chang, J. J. Hwang, F. B. Weng, S. H. Chan, *J. Power Sources* **2007**, *166*, 149–154; b) I. Nitta, T. Hottinen, O. Himanen, M. Mikkola, *J. Power Sources* **2007**, *171*, 26–36; c) J.-H. Lin, W.-H. Chen, Y.-J. Su, T.-H. Ko, *Fuel* **2008**, *87*, 2420–2424.

[22] T. Matsuura, M. Kato, M. Hori, *J. Power Sources* **2006**, *161*, 74 – 78.
[23] a) S.-D. Yim, B.-J. Kim, Y.-J. Sohn, Y.-G. Yoon, G.-G. Park, W.-Y. Lee, C.-S. Kim, Y. C. Kim, *Curr. Appl. Phys.* **2010**, *10*, S59 – S61; b) V. Mishra, F. Yang, R. Pitchumani, *J. Fuel Cell Sci. Technol.* **2004**, *1*, 2 – 9.
[24] H.-R. Jhong, F. R. Brushett, L. Yin, D. M. Stevenson, P. J. A. Kenis, *J. Electrochem. Soc.* **2012**, *159*, B292 – B298.

Manuscript received: July 11, 2017
Revised manuscript received: August 17, 2017
Accepted manuscript online: September 22, 2017
Version of record online: October 24, 2017